Measurement and calculation of polarization and potential-energy effects on core-electron binding energies in solids: X-ray photoemission of rare gases implanted in noble metals

P. H. Citrin and D. R. Hamann
Bell Laboratories, Murray Hill, New Jersey 07974
(Received 10 April 1974)

The binding energies of core electrons on Ne, Ar, Kr, and Xe implanted in Cu, Ag, and Au have been measured by x-ray photoemission and are found to be 2–4 eV smaller in magnitude than the corresponding binding energies obtained from gas-phase measurements. All implanted data have been referenced to the vacuum level of the appropriate metal and are therefore absolute energies suitable for gas-phase comparison. For a given noble-metal host, the magnitude of the binding-energy shift decreases monotonically from Ne to Xe, while for a given rare-gas core electron the shift is largest in Ag and smallest in Cu. Investigation of both these trends allows for the study of the two contributions responsible for these shifts. First, the self-consistent potential experienced by the core level is changed upon implantation (the initial state). Second, the polarization of metal-host electrons upon photoionization (the final state) provides relaxation energy not present in the free atom. Both these effects have been calculated using a model which represents the metal-host valence s electrons as free, the host outer d electrons as a dielectric, and the neutral and photoionized rare gas by a pseudopotential. The model is treated using a density-functional method that allows for both self-consistency and nonlinear screening by the host electrons. All the parameters in the model are empirically determined independently of the present experiment. The results show that the potential shift and polarization energy are of comparable magnitude and opposite sign, so that significant cancellation occurs. The calculated trends in total binding-energy shift for the series of gases in each metal are in excellent agreement with the experimental results, and the trends for each gas from metal to metal are reasonably well reproduced. An essentially uniform discrepancy of 1.4 eV between the absolute calculated and measured values is ascribed to limitations of the model and detailed knowledge of the implantation-site geometry.

I. INTRODUCTION

The technique of x-ray photoemission spectroscopy (XPS or ESCA) has progressed considerably since the discovery of the chemical-shift phenomenon in 1964.[1] New developments in x-ray monochromatization and sample-preparation procedures have enabled the measurements of binding energies of core electrons in solids,[2] gases and vapors,[3] molecular beams,[4] and even liquids,[5] to quite high accuracy and have allowed one to distinguish, in favorable cases, species in the same material that are energetically inequivalent by only several tenths of a volt.[6] Commensurate with these experimental developments has been a growing interest in the calculation of core-electron binding energies. The degree of sophistication required to adequately keep pace with existing data has similarly progressed from simple frozen-orbital (Koopmans's theorem[7]) calculations to calculations of self-consistent hole states.[8–22] These latter methods, while satisfactorily accounting for the polarization of the passive electrons by the core hole in the final state, are necessarily restricted to very simple systems such as atoms and ions[2,8–15] or small molecules.[16–22] The question of how one may calculate core-electron binding energies of atoms in solids to a reasonable degree of accuracy while not involving unreasonable computational time and difficulty is the subject of this paper. In order to appreciate the approach to this problem, it is necessary to outline briefly the major factors of consideration.

The first is the initial-state Hartree potential of the atom in the solid. Clearly it will be modified in going from the free species to the solid phase. This initial-state potential shift can, for example, be as large as tens of volts for a free ion being incorporated into an ionic crystal. Also, just as the magnitude and sign of the charge on the ion determine the sign of the shift (e.g., an electron in a free Ca^{++} ion is less bound in a CaF_2 crystal by ~20 eV while an electron in free F^- is more bound by ~11 eV in the same crystal), so can the different interactions of an atom with its solid host affect the magnitude and sign of this potential shift.

The second point to consider is a final-state effect. Whereas passive electrons are polarized in free atoms or ions upon formation of a hole state, passive electrons from the surrounding solid environment may also be polarized. Here the effect is always a lowering of the absolute magnitude of the binding energy because, from energy conservation, the photoejected electron acquires the energy lost from the passive electrons being polarized towards the region of more attractive potential. The significance of this effect in x-ray photoemission was first appreciated by Hedin,[23] who calculated

from linear-response theory polarization energies of conduction electrons in free-electron-like metals. The effects and calculations of polarization energies were later shown to be important in x-ray photoemission measurements of ionic crystals,[24] even though the passive electrons on the surrounding ions are highly localized.

The final factor to consider is the problem of choosing a suitable and meaningful reference level. For pure metals in electrical contact with the spectrometer, the Fermi level is a logical choice. Knowledge of that metal's work function can, in principle, determine its vacuum level as well. For alloys, this becomes less practical due to a lack of work-function data. For insulators or semiconductors under x radiation, the problem is further complicated because the Fermi level in such a nonequilibrium condition is not well defined.[24(b)] Also, these samples may accumulate excess charge and modify the core levels further still.

Realizing the significance of the above-mentioned factors, the system chosen in order both *experimentally and theoretically* to isolate them in a systematic and well-definable manner was that of implanted rare gases in noble metals. The rare gases, being closed-shelled atoms and thus chemically inert, are minimally affected by implantation. Since accurate XPS data exist for these free gases, it is then possible to isolate any effects produced by the host solid in a way consistent with the monotonic variations in the gas atom's size. The noble metals are attractive hosts for a variety of reasons. They are isostructural and isoelectronic with nonmonotonic lattice constants and work functions, thereby readily lending themselves to systematic investigation. Being metals whose work functions are accurately known eliminates the reference-level problem, provided the surface purity of the metals is sufficiently high to ensure implantation into the metal. In this regard, the noble metals are ideal due to their relative chemical inertness and thus their ability to be cleaned and to remain clean during the course of the experiments. Lastly, the essentially quasifree conduction s electrons in these metals permit itinerant-electron assumptions in the calculation of their response to the photoionized rare-gas atom. Thus, it is seen that through comparison of free and implanted rare-gas electron binding energies as a function of rare gas and metal host, it is possible to study trends in *both* the initial-state potential changes and the final-state polarization processes.

Results of the x-ray photoemission measurements are presented in two parts in Sec. III. The first contains a summary of conclusions regarding the line shapes of the implanted photopeaks and their relationship with linewidth and radiation effects. A more detailed discussion of pertinent line-shape information is given in Appendix A. The second part of Sec. III compares the measured binding energies of implanted rare-gas core electrons with those of the corresponding free gases to obtain the empirical binding-energy shifts. Section IV, also in two parts, describes first an outline of the theoretical model and, secondly, the appropriate choice of model parameters used to calculate the binding-energy shifts. Details of the method of solution employed in these calculations are given in Appendix B. In Sec. V, results of the calculations are compared with experimental results and implications of the agreement are discussed.

II. EXPERIMENTAL PROCEDURES

Rare-gas ions of 1.0 keV were implanted into high-purity polycrystalline metal samples with a conventional ion-sputtering gun. Rather high ion doses, typically $\sim 10^{16}$ ions/cm^2, ensured that the concentration of rare-gas atoms reached a level of saturation. This was confirmed by channeling experiments which are described in Appendix A. Further discussion there is also given to the gas concentration, range, damage, and lattice location of the implanted ions.

The data used to determine the binding-energy shifts were taken with a Varian IEE spectrometer using Mg $K\alpha$ radiation.[25] In this instrument the working pressure was never greater than 2×10^{-8} Torr. The surface purity of the metal hosts was monitored before and after the sputtering procedure, which served to clean the metals as well as to implant the atoms. Immediately after sputtering, oxygen contamination was not at all perceptible in any of the metals. As a further check on the possible effects of surface purity on these implantation measurements, several measurements of various implanted gases were repeated using a Hewlett-Packard 5950A ESCA spectrometer in which the working pressure was $\sim 10^{-9}$ Torr. Here, as before, oxygen contamination was observed to be negligible. Comparison of the binding energies for both the host and implanted-gas electrons with those obtained in the somewhat poorer vacuum showed them to be in agreement to within 0.15 eV, even for those gases implanted in the comparatively more reactive Cu metal. The importance of these results is that implantation in the metal—not in a surface contamination layer on that metal—is clearly established. While recognizing that work functions are sensitive to submonolayer coverages, it should be emphasized that such *work-function changes due to surface impurities are immaterial to the problem of choosing a suitable reference level for the metal, so long as the metal is in electrical contact with the spectrometer.* Further discussions of reference levels are given in Appendix B.

III. RESULTS

A. Line shapes

The rare-gas core levels studied most in this investigation were Ne $1s$, Ar $2p_{3/2}$, Kr $3p_{3/2}$, and Xe $3d_{5/2}$ because they were the most intense. Other weaker core levels gave essentially identical binding-energy shifts, and these are discussed in Sec. III B. In addition to the energy shifts, noteworthy line-shape features were observed for the core levels of the implanted gases and these features were twofold. The first was a considerable line broadening compared with widths of corresponding lines observed in spectra of free gaseous atoms. The second was a noticeable line asymmetry which was observed only for Ne $1s$ electrons implanted in all three metals. Possible causes for these results may be lifetime effects or effects associated with multiple implantation sites in the lattice. Both possibilities are considered separately and in some detail in Appendix A. The conclusions of that discussion which are pertinent to our analysis of binding-energy shifts are summarized below.

(i) Core-electron linewidth broadening of implanted rare gases is not due to hole-state lifetime variations arising from chemically dependent Auger transition rates. The exact source of the broadening is presently unexplained.

(ii) The average range of implanted atoms is between 10 and 20 Å, comparable to mean escape depths for photoelectrons analyzed in these experiments.

(iii) A steady-state concentration of implanted atoms is reached in these experiments, which amounts to about 1% total implant concentration.

(iv) For Ar, Kr, and Xe, "substitutional" implantation associated with only a small fraction of nearest-neighbor vacancies appears to describe aptly the average configuration for each implant site; for Ne implantation, such a description is also applicable, but small clusters are apparently formed in addition.

B. Binding-energy shifts

As stated, the bulk of the data used in this work were obtained with a Varian IEE spectrometer and similar spectra from it have already been presented in a preliminary report.[25] Typical spectra for Ne and Xe implanted in Cu taken with a HP 5950A ESCA spectrometer are given in Appendix A. The Varian data, in which all cases of gases implanted in metals were run at least twice, are reproducible to better than 0.15 eV. In those cases for which comparison with the HP data is possible, similar reproducibility was obtained. Data from both instruments were analyzed with a nonlinear least-squares fitting procedure using line shapes adjustable between Gaussian and Lorentzian. Except for the case of neon, all data were fitted with one peak. For Ne, the strong asymmetry observed suggested at least a two-peak fit. Discussion in Appendix A of the cause for this asymmetry further suggested the use of only the more-intense lower-binding-energy component for Ne in our analysis.

The binding energies determined from the fits are listed in Table I under E_B^F(impl) and are the average values for all the runs. The errors, in parentheses, calculated by statistical laws, include the deviations from the mean value as well as the standard deviations from the fitting procedure. The superscript notation E_B^F(impl) refers to the Fermi level of the metal host which was used as the zero-binding-energy reference.

If we compare the binding energies E_B^F(impl) with the corresponding binding energies in the free gaseous atom E_B^V(gas), it is seen that the former values are considerably smaller in magnitude. (We remind the reader that in this and other discussions, binding energies shall be discussed in terms of absolute magnitudes, e.g., $1s$ electrons have higher binding energies than $2s$ electrons.) The superscript for the values of E_B^V(gas), which were taken from Siegbahn *et al.*[3] and Johannson *et al.*,[26] denotes the vacuum reference level. Values of the experimental binding-energy shift Δ_{expt}^F, defined by

$$\Delta_{\text{expt}}^F = E_B^V(\text{gas}) - E_B^F(\text{impl}), \tag{1}$$

are given in the middle column of Table I. Here, the uncertainties, in parentheses, also include those associated with E_B^V(gas).[3,26] We have plotted Δ_{expt}^F for the different noble metals and gases in Fig. 1(a). Before discussing these results it must be realized that because different reference levels

TABLE I. Summary of data (in eV).[a]

Host	Gas	E_B^F(impl)[b]	Δ_{expt}^F[c]	Δ_{expt}^V[c]
Cu	Ne	862.18(4)	8.19(11)	3.54(12)
	Ar	241.09(7)	7.53(11)	2.88(12)
	Kr	207.27(6)	7.28(16)	2.63(17)
	Xe	669.58(2)	6.82(15)	2.17(16)
Ag	Ne	862.38(10)	7.99(13)	3.99(20)
	Ar	241.19(3)	7.43(11)	3.43(19)
	Kr	207.60(5)	6.95(16)	2.95(22)
	Xe	669.62(12)	6.78(19)	2.78(24)
Au	Ne	861.56(7)	8.81(10)	3.71(19)
	Ar	240.26(4)	8.36(9)	3.26(17)
	Kr	$-d$	...	...
	Xe	668.89(8)	7.51(17)	2.41(23)

[a]Numbers in parentheses represent uncertainties in last digit(s).

[b]Binding energy measured relative to Fermi level of host.

[c]Defined in text.

[d]Kr could not be successfully implanted in Au.

TABLE II. Implanted-rare-gas cavity radii, crystal radii, and van der Waal's radii (in A).

Gas	in Cu[a]	in Ag, Au[a]	Crystal[b]	Lennard-Jones[c]
Ne	1.81	1.91	1.60	1.57
Ar	2.09	2.17	1.92	1.92
Kr	2.18	2.29	2.02	2.02
Xe	2.30	2.40	2.21	2.27

[a]This work.

[b]R. G. Wyckoff, *Crystal Structures*, 2nd ed. (Interscience, New York, 1963), Vol. 1.

[c]J. O. Hirschfelder, C. F. Curtiss, and R. B. Bird, *Molecular Theory of Gases and Liquids* (Wiley, New York, 1954).

are used to determine Δ^F_{expt}, these are not very physically meaningful numbers. It is therefore desirable to use a common reference, which we take as the vacuum level. (This point is discussed further in Sec. IV B and Appendix B.) Since

$$E_B^V(\text{impl}) = E_B^F(\text{impl}) + W_M \tag{2}$$

where W_M is the work function of the metal sample, the binding-energy shift to be studied is Δ^V_{expt},

$$\Delta^V_{\text{expt}} = E_B^V(\text{gas}) - E_B^V(\text{impl}). \tag{3}$$

The shifts Δ^V_{expt} were determined using Eastman's values of W_M for clean polycrystalline Cu, Ag, and Au which are, respectively, 4.65 ± 0.05, 4.0 ± 0.15, and 5.1 ± 0.1 eV.[27] These shifts are given in the last column in Table II and are plotted in Fig. 1(b). The sole purpose for introducing Δ^F_{expt} is to emphasize the importance of selecting appropriate reference levels and to illustrate the various sources of uncertainty introduced in determining Δ^V_{expt}.

IV. CALCULATION OF BINDING-ENERGY SHIFTS

A. Theoretical model

In choosing a theoretical method appropriate to the goals of this investigation, several considerations influenced our decision. First, it was decided that direct calculations of the core levels in a solid environment could not be carried out with sufficient accuracy to give a useful comparison with chemical trends in a series of measurements. This suggested that the largest closed-shell (rare-gas atom or metal ion) configuration be used as a reference, whose core level energies could be determined experimentally. Only changes in these energies due to electrons outside the closed shell would be calculated.

The fact that only the valence electrons were to be explicitly considered in the calculations strongly suggested the usefulness of pseudopotentials in describing the interactions of the reference closed-shell core with valence electrons.[28] Wide experience with pseudopotentials in solid-state calculations has indicated that a pseudopotential whose parameters are adjusted to fit the energy levels in one situation, say a particular solid or the atom, does a good job in all other situations. This transferability of pseudopotentials makes them particularly suited to the questions of binding-energy shifts addressed here.

The second major decision required was how to calculate the response of the valence electrons, which in the cases considered were conduction electrons in metals. The possibility of a full self-consistent quantum-mechanical calculation was dismissed, since this would be comparable to such a calculation for a realistic model of an impurity, and the state of the art in this area is not very advanced. The simplest alternative considered was the use of linear-response theory, which has been applied to this problem in the past.[23] This method, however, gives a distribution of screening charge for the photoionized atom that depends only on the average conduction-electron density, and therefore neglects most of the effects which can give rise to the chemical trends in the shifts in a given series.

A second method which has been applied makes use of atomic wave functions for the screening charge, extending a method developed for free atoms[29] to the case of atoms in metals. The screening charge is considered to occupy the lowest unoccupied wave function calculated for the atom one to the right of the photoexcited atom in the Periodic Table.[30,31] While this latter method builds in details of the screening cloud near the nucleus more

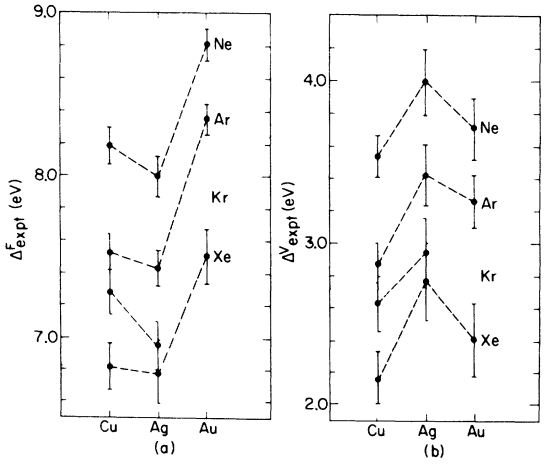

FIG. 1. (a) Experimental binding-energy differences between gaseous and implanted rare-gas core electrons. The Fermi and vacuum levels are the zero-binding-energy references for the implanted and gaseous atoms, respectively. (b) Absolute experimental binding-energy differences, using common vacuum-level reference.

accurately than linear-response theory, it gives a number that is independent of the chemical environment of the photoexcited atom—the only role played by the host is that of an electrical conductor capable of supplying the additional electron. This method also fails to provide a means of calculating the shift in binding energy due to the change in initial-state potential at the core produced by the compression of the valence wave functions in going from the atom to the solid.

The most suitable compromise, it was decided, was to apply a density functional method. In such a calculation, the total energy of a system is expressed as a functional of the electron density $n(\vec{x})$, and the density is varied, subject to a constraint on the total number of electrons, to achieve the minimum value of the functional.[32] The interactions of the electrons with an external potential and the average electron-electron Coulomb interactions are, of course, exactly expressed as functionals of the density. The quantum-mechanical quantities such as the zero-point kinetic energy, the exchange energy, and the correlation energy can only be approximated by a density functional. One such approximation, which has been widely used in atoms, has recently been shown to give good results when used in combination with pseudopotentials for the lattice constants and compressibilities of a large number of solids.[33] This is known as the Fermi-Thomas-Dirac-Weizsäcker method.

The total energy in this approximation can be written

$$E = \int f[n(\vec{r})]\, d\vec{r} - \tfrac{1}{2}e\int [n(\vec{r}) - n_+(\vec{r})]\, V_e(\vec{r})\, d\vec{r}, \quad (4)$$

where $n(\vec{r})$ is the electron density, $n_+(\vec{r})$ is the distribution of positive charge (assumed fixed), V_e is the electrostatic potential, and f represents the remaining energy terms. We follow the convention that V_e is electrostatic potential, so that the potential energy felt by an electron is $-eV_e$, where e is the magnitude of the electronic charge. With this convention, V_e is given by the solution of Poisson's equation

$$\nabla^2 V_e(\vec{r}) = 4\pi e[n(\vec{r}) - n_+(\vec{r})]. \quad (5)$$

The function f has the form

$$f = c_k n^{5/3} + \frac{c_w}{4}\frac{|\vec{\nabla} n|^2}{n} - c_e n^{4/3} - enV_{ps}, \quad (6)$$

where $c_k = \frac{3}{10}(3\pi^2)^{2/3}\hbar^2/m$, $c_w = \hbar^2/2m$, and $c_e = \frac{3}{4}(3/\pi)^{1/3}e^2$. The $n^{5/3}$ term is the leading kinetic-energy term, based on a uniform electron gas, and the $\vec{\nabla} n$ term is the von Weizsäcker correction which represents the extra cost in kinetic energy necessary to have the density vary rapidly.[34] The $n^{4/3}$ term represents the exchange and correlation energy, and the V_{ps} term, the interaction with the pseudopotential.

In the x-ray-absorption process, we single out the atom which is photoionized. The induced screening charge in the final state, which is responsible for the relaxation energy, will be localized near this atom. It is clear that we must take the pseudopotential of this atom accurately into account if we wish to describe trends in the relaxation energies. The remaining atoms in the solid have less contact with the screening cloud, however, and their pseudopotentials should have less effect. This suggests that it should be a good approximation to replace all but the photoexcited ion by a uniform positive background, the so-called jellium model. Of course, an appropriate amount of positive background must be excluded from the vicinity of the atom whose potential we treat in more detail, to avoid double counting. A spherical cavity of radius R_0 is introduced for this purpose. This approximation makes possible a spherically symmetric geometry, and greatly simplifies the variational problem of finding the density, which minimizes the energy functional.

For the case of the noble metals, Cu, Ag, and Au, it is not clear that the jellium characterization is entirely adequate. The d states, while completely filled, lie near the Fermi energy and are polarizable. They could thus produce a significant polarization energy even in the absence of mobile screening charge. To approximate this effect, a uniform dielectric is assumed to exist coincident with the positive background. The Coulomb-interaction part of the energy functional must be suitably modified to take this into account. This can be done by dividing the right-hand side of Eq. (5) by the dielectric constant ϵ_d for $r > R_0$. The boundary conditions on V_e at R_0 are given by the usual rules of elementary electrostatics at dielectric surfaces, and Eq. (4) remains the correct expression for the energy. We have not modified the exchange-correlation term to include the dielectric on the grounds that the long-range zero-frequency d-band dielectric function is not appropriate to the short-range and large virtual energy transfers associated with these processes among the s electrons. A more sophisticated treatment of this question is certainly beyond the purview of the present study. Values for the interband dielectric constant ϵ_d in Cu and Ag have been extracted from optical and ultraviolet spectroscopic measurements and are discussed in Sec. IV B.

Two pseudopotentials must be chosen to represent the rare-gas atom, one for the initial ground state and a second for the photoionized state. The rare-gas atom with a core hole is analogous to an alkali ion, and for this case the simplest choice is the Ashcraft pseudopotential[35]

$$V_{ps}(r)=\begin{cases}0, & r<R_c\\ e/r, & r>R_c,\end{cases} \tag{7}$$

where the single fitting parameter R_c can be loosely interpreted as the core radius. This form of pseudopotential has been used successfully in combination with the functional method adopted here.[33] The presence of the dielectric for $r>R_0$ modifies V_{ps} from its conventional form given above, and we instead must use the expression

$$V_{ps}(r)=\begin{cases}-(e/R_0)(1-1/\epsilon_d), & r<R_c\\ e/r-(e/R_0)(1-1/\epsilon_d), & R_c<r<R_0\\ e/\epsilon_d r, & R_0<r.\end{cases} \tag{8}$$

For the initial state of the rare-gas atom, we expect a short-range repulsive pseudopotential. We believe that the best simple choice is a "soft-core" square barrier. While the height and radius of this barrier could be chosen independently, we have simplified this pseudopotential to contain only a single parameter by relating the barrier height and the core radius in the same way as they are related for the Aschroft potential,

$$V_{ps}(r)=\begin{cases}-e/R_c, & r<R_c\\ 0, & R_c<r.\end{cases} \tag{9}$$

B. Model parameters

The calculations described in Appendix B have been carried out for rare-gas atoms implanted in Cu, Ag, and Au. The parameters needed for each calculation are the pseudopotential parameters, the effective cavity radius, the average electron density, and the interband dielectric constant.

Free rare-gas atoms act on low-energy electrons as repulsive hard-core scatterers with a weak but long-range attractive tail due to induced polarization. The interaction of these two factors dominates in scattering experiments. In a metal, the weak attractive tail will be negligible because of screening, and only the repulsive core will be important. This term may be isolated by looking at Hartree-Fock calculations of electron–rare-gas scattering.[36] These calculations have been carried out for Ne and Ar, but not for Kr and Xe. For the photoionized atoms, of course, no such calculations exist. It is reasonable to assume, however, that a rare-gas atom with a core hole will act much as the ion of the corresponding alkali metal to its right in the Periodic Table. Ashcroft "core" radii R_c have been obtained describing all these ions from solid-state data, and we use the values 0.88, 1.12, 1.44, and 1.55 Å for Na, K, Rb, and Cs, respectively.[28]

The neutral-rare-gas model potential, Eq. (9), was fitted to the Hartree-Fock scattering calculation for Ne and Ar. The core radii obtained in this manner were within 4% of the corresponding alkali core radii in both cases. This correlation was considered sufficiently good to use the potential in Eq. (9) with the alkali Ashcroft radii to represent all the neutral rare gases. We did not make the small corrections required to adjust the neutral model radii to exactly fit the scattering calculation for Ne and Ar since we could not make corresponding corrections for Kr and Xe.

The choice of radii R_0 for the spherical cavities in the positive background was not straightforward for the implanted rare gases. Simply using the Wigner-Seitz radius of the metal atom gave an unphysically small number. On the other hand, using a radius based on the rare-gas atom alone fails to account for the fact that a given atom produces a larger strain in Cu than in Ag or Au, and therefore should produce a relatively smaller cavity. It was felt that a better estimate could be obtained by using the rare-gas–alkali analogy further, and examining data on low-concentration alloys of alkalis in the noble metals. We found that only Au dissolved all the alkalis, and that each alkali atom expanded the lattice considerably.[37] We chose a jellium cavity volume equal to the effective volume per alkali atom in the dilute limit. This should give a slight underestimate, since the neutral rare gas is more repulsive than the alkali, but the discrepancy is surely beyond the absolute accuracy of the model.

For the other cases, data existed only for Na in Ag, and its effective volume was essentially equal to that of Na in Au. For the remaining cases, we devised a one-parameter empirical scaling law

$$v_{12}=v_1^{1-\alpha}v_2^{\alpha}, \tag{10}$$

where v_{12} is the effective volume of the alkali in the alloy, v_1 is the atomic volume of the pure alkali, and v_2 is the atomic volume of the noble metal. The choice $\alpha=0.36$ fit the Au data well, and this formula was used to generate the volumes for Cu. Since v_2 is the same for Au and Ag, the same volumes were used for both. The corresponding cavity radii are given in Table III. It is interesting that these empirically determined cavity radii do turn out to be similar to the experimental crystal and theoretical van der Waal's radii; these latter values are also given in Table II for comparison.

The contribution of the filled d shell to the static dielectric constant ϵ_d for Cu and Ag was deduced from optical and ultraviolet absorption measurements.[38] Because these data were not available for Au, an empirical procedure was devised to estimate ϵ_d. The dielectric constant can be represented by the expression

$$\epsilon_d = 1 + \hbar\omega_p / E_g, \tag{11}$$

where ω_p is the free-electron plasma frequency for the average density of the electrons in question, and E_g is an average interband energy gap.[39] Equation (11) is best regarded as a definition of E_g. We calculated E_g for Cu and Ag from the published ϵ_d values, and noted that this energy was approximately four times larger than that of the first peak in the interband absorption spectrum.[38] This much of the spectrum is available for Au,[40] so the same relation was assumed to hold. The deduced d-band dielectric constants are given with the others in Table III.

As discussed in Appendix B, the "natural" reference level for the theoretical calculation is the average internal electrostatic potential of the host. To compare this reference energy with an experimentally meaningful reference energy, it was decided to use the vacuum level, which involves computing the surface dipole, rather than the Fermi level. There are two reasons for this choice. First, the effects of the s-d hybridization in these metals makes the relation between the Fermi level and the average internal potential a very difficult quantity to estimate. Certainly the jellium result is not valid for this quantity. Second, the cavities around the rare-gas atoms are rather large, so a substantial fraction of the dipole that would form at a free surface forms between the metal and the rare-gas atom. Therefore, errors in computing the vacuum potential relative to the internal potential (i.e., the free surface dipole) should at least partially cancel against corresponding errors in computing the initial-state energy of the rare-gas core level relative to the average internal potential. The dipoles were calculated using exactly the same theoretical methods, and in fact the same computer program. The rare-gas atom was simply removed from the cavity, and the cavity radius R_0 was allowed to become large. The potential at the cavity center then asymptotically approached the vacuum potential. The calculated dipoles are given in Table III.

The dipoles we calculated are significantly larger than those of Lang and Kohn for the noble metals.[41] There are several reasons for this discrepancy. First, the density functional method used here is less accurate for the kinetic energy than the complete self-consistent solution of Schrödinger's equation carried out by Lang and Kohn. Second, a simpler expression for the exchange and correlation potential is used here. Finally and perhaps most importantly, the model used here differs through the inclusion of the d-band dielectric response ϵ_d. Dipoles calculated with actual ϵ_d values were (20–30)% larger than dipoles calculated with $\epsilon_d = 1$.

TABLE III. Conduction-electron Wigner-Seitz radius r_s, d-band dielectric constant ϵ_d, and calculated surface electrostatic dipole potential D.

Metal	r_s (Å)	ϵ_d	D(eV)
Cu	1.41	4.6[a]	5.9
Ag	1.59	2.4[a]	4.6
Au	1.59	3.3	4.6

[a]Reference 38.

The calculations we have described were carried out for each pair of implanted gas and host for the initial state (repulsive pseudopotential) and final state (Ashcroft pseudopotential). The self-consistent charge densities which minimize the energy functional in the initial and final states are illustrated by the case of Ne implanted in Cu shown in Fig. 2. It was observed that the results were about comparably sensitive to similar changes in the parameters r_s, R_c, and R_0. Actual values of R_c and R_0 tended to be correlated since both are increasing functions of the size of the implanted atom. The results were less sensitive to changed in ϵ_d in the range spanned since the relevant parameter is really ϵ_d^{-1}, which was small in all cases. The results for the binding-energy shifts, broken down into polarization energy and potential-shift contributions, are shown in Fig. 3.

V. DISCUSSION

The primary goal of this work was to investigate systematically the factors responsible for determining the binding energy of electrons on atoms in solids. These factors have been classified into two terms: the initial-state potential and the final-state polarization energy. Although it has been shown in Appendix B that this separation is unnecessary for the actual calculation of binding energies in solids, we shall continue to discuss the results of our analysis along these lines because a valid physical distinction exists between the two effects.

A comparison of the experimental binding-energy shifts referenced to the vacuum level, Δ^V_{expt}, and the calculated shifts referenced to the same level, Δ^V_{calc}, are summarized in Table IV and shown in Fig. 4. On the first level of comparison, we see that the calculated *relative* shifts for different rare gases in a given metal host are in excellent agreement with the experimental values. For ten of the eleven cases studied (Kr in Cu not included), the calculated shifts are in agreement to within ~0.3 eV. The mean of the discrepancies between the calculated and experimental shifts is only 0.19 ± 0.13 eV for these ten cases and only 0.25 ± 0.21 eV for all eleven. The significance of this result is that it puts on firm ground our choice of

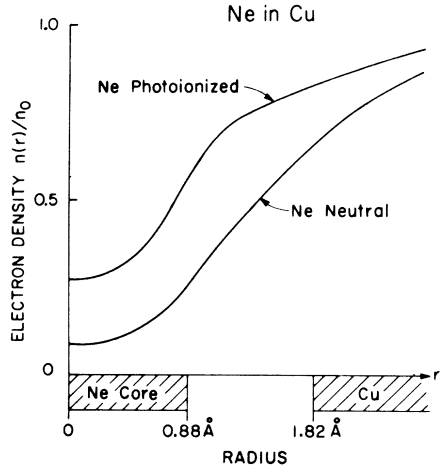

FIG. 2. Copper conduction-electron density before and after photoionization of Ne 1*s* electrons. The integrated difference between the two curves is one electron.

TABLE IV. Comparison of experimental and calculated binding-energy shifts Δ^V (in eV).

Host	Gas	Δ^V_{calc}	Δ^V_{expt}	$\delta\Delta$
Cu	Ne	2.29	3.54	1.25
	Ar	1.60	2.88	1.28
	Kr	0.71	2.63	1.92[a]
	Xe	0.61	2.17	1.56
				1.36 ± 0.14
Ag	Ne	2.56	3.99	1.43
	Ar	1.98	3.43	1.45
	Kr	1.19	2.95	1.76
	Xe	1.06	2.78	1.72
				1.59 ± 0.17
Au	Ne	2.54	3.71	1.17
	Ar	1.95	3.26	1.31
	Kr	1.19	...[b]	
	Xe	1.04	2.41	1.37
				1.25 ± 0.11
				$\overline{\delta\Delta}$ = 1.40 ± 0.17

[a]This value not included.
[b]Kr could not be successfully implanted in Au.

model potentials for the rare-gas atoms and ions and for the sizes of the implantation cavity radii used in the calculations.

The physical interpretation of the actual trend in relative binding-energy shifts may be understood through inspection of Fig. 3, in which the polarization-energy trends are seen to be more important than those of the potential-energy shifts in a given host. This is perhaps not surprising, for it is expected that the smaller Ne cavities should allow a more compact screening cloud than the larger Xe cavities, and that this effect should dominate differences in cavity "surface" dipoles. The trend with cavity size can be understood semiquantitatively in terms of a simple image-potential model. If the internal "surface" of the metal-host cavity is replaced by an ideal conducting sphere of slightly smaller radius,[42] R_{eff}, classical electrostatics gives the relaxation energy as $e^2/2R_{eff}$, which compares well with the results of our detailed calculation. To understand the smallness of the changes in initial-state potential, we note that the cavity radii are several times the characteristic decay length of the charge at a free metal surface of similar electron density. Therefore if the cavity were empty, the potential would nearly reach the vacuum level. The presence of the repulsive rare-gas atom makes the buildup of surface dipole at the cavity surface less complete, but the repulsive model potential is relatively small compared to the cavity radius, and much of the dipole remains.

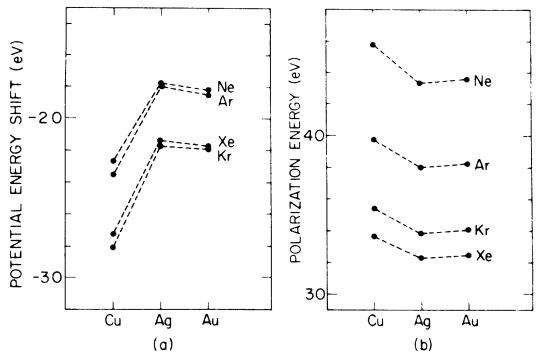

FIG. 3. Polarization and potential-energy contributions for the implanted gases in the noble metals. The potential shift is the change in the *initial*-state Hartree potential of the core levels due to implantation in the metal host, and tends to increase the magnitude of the binding energies. The polarization energy is the apparent decrease in the magnitude of the binding energies due to the response of the host electrons to the presence of the *final*-state core hole.

On the second level of comparison of theory and experiment, we look at the *absolute* values of the binding-energy shifts. This comparison, given in the last column of Table IV, shows the calculated values for all cases to be smaller than experimental shifts by an essentially constant amount. The mean discrepancy of all shifts is 1.40 eV, with the rms of this deviation being only ± 0.17 eV. There are two physical effects that have been neglected which could give rise to such systematic error. The first is the intrinsic limitation of the jellium model for the description of the noble metals.[41] While the approximate inclusion of the *d*-band

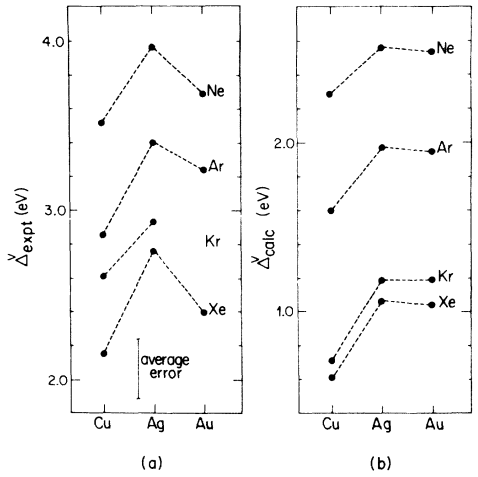

FIG. 4. Comparison between experimental absolute binding-energy shifts and total calculated shifts. The absolute scale of (b) is offset from that of (a) by 1.40 eV.

polarizability corrects one defect of simple jellium, the omission of s-d admixture is undoubtedly serious. Our model tends to overestimate the work function, and presumably the surface dipole. Since the potential contribution to the binding-energy shift can be considered a fractional change in dipole between a real surface and the cavity "surface," a decrease in the magnitude of the dipole would improve agreement. The second effect is the possible changes in the outermost rare-gas wave functions. We have included the repulsive interaction between these and the host conduction electrons, but only permitted the conduction electrons to respond. Since the rare-gas electrons are not, in fact, perfectly rigid, they would be expected to compress slightly. This would increase the intraatomic Coulomb interactions in the initial state, and therefore decrease the magnitude of the binding energy. The concomitant increase in the intraatomic relaxation would also be in the right direction, but undoubtedly small compared to the initial-state effect. In light of the uncertainties about the detailed atomic arrangement near the implantation site, the considerable computational effort involved in attempting to remove these sources of systematic error seems unwarranted at present.

The final comparison of experiment with theory is seen from inspection of the relative trends for a given rare-gas atom in different metal hosts, shown in Fig. 4. From this figure it is seen that the nonmonotonic trend of shifts in going from Cu to Ag to Au is reasonably reproduced by the calculations, although somewhat less satisfactorily for Ag to Au. The reason for this is obvious from Fig. 3(b), in which it is seen that the potential shifts for Ag and Au are calculated to be about equal due to their similar lattice constants. However, it is known that their work functions, which are in large measure determined by their surface dipoles, are different by as much as 1 eV.[27] The surface dipoles of these metals presumably differ this much because of differing s-d admixture, a phenomenon beyond the scope of our model. It is significant, however, that the most dramatic change in surface dipole between Cu and (Ag, Au) *is* reproduced. The physical basis of this is simply the greater conduction charge density due to the smaller lattice constant of Cu. The point to stress here is that if we had simply considered the polarization energies and did not include the potential shifts—however crudely calculated—the trend of calculated shifts would be in the exact opposite direction from that experimentally observed. Furthermore, the calculated shifts in the absence of potential considerations would overestimate the observed shifts. Thus, the importance of considering *both* initial- and final-state effects is clearly demonstrated.

A general assessment of the agreement of our theory with experiment shows it to be quite satisfactory. This becomes particularly clear when it is realized that the theoretical values represent *differences* between larger numbers coming from separate effects whose magnitudes, in some cases, are of comparable value. It should further be realized that the relative degree of agreement, of the order of tenths of volts, is most gratifying, especially in view of the uncertainties inherent in the experiment itself and the consequent uncertainties imposed in the choice of model parameters. (Recall that all model parameters were determined by data entirely independent of the present experiments.) Perhaps most significantly, our method includes both initial- and final-state effects on core-electron binding energies through calculations that are both physically reasonable and computationally expedient. This fact, coupled with its inherent feature of treating the nonlinear response of the polarized electron medium, makes this method nicely suited for systems in which the interactions of atoms with solids are better defined. Examples of this will be treated in a separate work.[43]

ACKNOWLEDGMENTS

The authors are indebted to W. L. Brown for performing the channeling experiments and for stimulating discussions with him and L. C. Feldman on radiation-damage effects. We also thank T. X. Carrol and T. D. Thomas for their assistance in obtaining the xenon-gas data. We gratefully acknowledge S. Hüfner and G. K. Wertheim for their initial work on implanted gases which stimulated this investigation.

APPENDIX A: LINE SHAPES OF IMPLANTED-RARE-GAS CORE ELECTRONS

Lifetime effects

The mechanism primarily responsible for decay of core hole states bound by $\gtrsim 1$ keV is emission of Auger electrons.[44] It has been recently shown that the lifetimes of core hole states which decay via Auger transitions involving valence electrons on the hole-state atom in question depend on the chemical nature of that atom.[45,46] Since the noble-gas atoms have closed-shell configuarations, it would be expected that the chemical nature of their valence shells, and thus the lifetimes of their valence and penultimate (i.e., least-bound core) levels, would be little affected by implantation. An alternate Auger mechanism that has been recently discussed involves transitions from valence electrons associated with nearest-neighbor ligands to the hole-state atom.[47] In the case of implanted rare-gas atoms, the interatomic transitions of most importance would involve the decay of rare-gas valence hole states V_{RG} by annhilation and ejection of metal valence electrons V_M; in Auger notation this is denoted by $V_{RG}V_M V_M'$. For a rare-gas penultimate-core hole state C_{RG}, interatomic transitions of the type $C_{RG}V_{RG}V_M$ might occur, although simple intra-atomic processes $C_{RG}V_{RG}V_{RG}$ would be expected to dominate since the rare-gas electron configuration is closed shell. *In principle,* it should be possible to test the importance of interatomic effects through XPS linewidth analyses of valence and penultimate levels. Unfortunately the intensity of the rare-gas valence electrons are quite small and, more importantly, their detection upon implantation is obscured by the metal d bands. On the other hand, the penultimate levels in the rare gases, viz., Ne $1s$, Ar $2p_{3/2}$, Kr $3d_{5/2}$, and Xe $4d_{5/2}$, do not suffer from these experimental difficulties, so the following test was performed.

The linewidths of both the Xe $4d_{5/2}$ and Xe $3d_{5/2}$ levels were measured in the gaseous and implanted cases. These levels were chosen because both are intense enough to obtain good statistics in reasonable counting times. The implanted xenon was studied in copper metal because there was no obstruction of the xenon core levels by those of that host. Gas-phase date for Xe were taken with a nonretarding electrostatic cylindrical mirror analyzer using Al $K\alpha$ radiation,[48] while the implanted data were taken with the HP 5950A ESCA spectrometer using monochromatized Al $K\alpha$ radiation. These latter data are shown in Fig. 5. The total measured linewidths, as determined from least-squares fits, and the widths of the lines after removing the instrumental and incident radiation widths[49–53] are compared for both sets of data in Table V. The errors in parentheses represent the

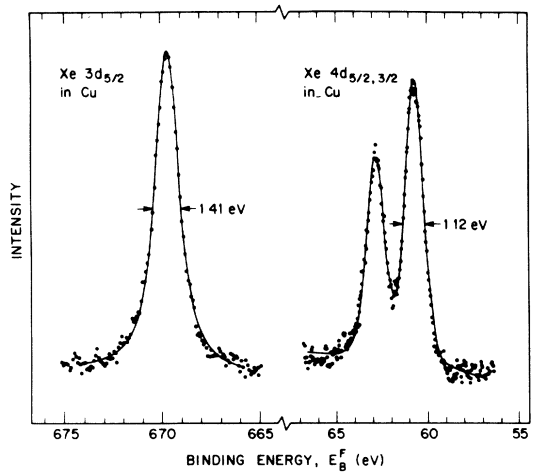

FIG. 5. X-ray photoemission spectra of core levels of xenon implanted in copper. The linewidths at full width at half-maximum were determined by least-squares fits and include instrumental and other broadening contributions.

uncertainties associated with the fitting and instrumental subtraction procedures.[49]

Inspection of the intrinsic widths for the gas-phase data show the Xe $3d_{5/2}$-hole width to be broader than that for Xe $4d_{5/2}$-hole, as expected. While this trend is also observed for the "intrinsic" widths of the implanted gases, we see that the Xe-$3d$–Xe-$4d$ width difference is much smaller and that, more importantly, both these "intrinsic" widths are significantly broader than those in the gas phase. This result, it should be noted, is relatively insensitive to minor changes in the assumptions used in the instrumental subtraction procedures.[49] Since lifetime effects should have little affect on the deeply bound Xe $3d$ levels, nonlifetime broadening mechanisms present in the implanted case but absent in the gaseous case are strongly suggested.

We may estimate the magnitude of this additional broadening by assuming that it is Gaussian (it is not lifetime related) and by assuming that the intrinsic widths determined from the gas-phase data are applicable to the implanted atoms. Using procedures discussed in Ref. 49, the total Gaussian component (including the Gaussian instrumental contribution) is determined; subtracting the instrumental width from this then gives the additional Gaussian broadening which is set out in the far left-hand column of Table V. We see that this latter contribution, of the order of 0.8–0.9 eV, is larger than the intrinsic widths of either core vacancy and is about the same magnitude for both levels. One possible source for this broadening

TABLE V. Linewidths of gaseous and implanted Xe (in eV).[a]

	Gas[b]		Implanted[c]			
Electron	Expt[d]	Intrinsic[e]	Expt[d]	"Intrinsic"[e]	Gaussian[f]	Additional[g]
Xe $4d_{5/2}$	1.37(4)	0.10(9)	1.12(3)	0.79(6)	1.06(10)	0.89(14)
Xe $3d_{5/2}$	1.52(2)	0.65(10)	1.41(2)	1.14(4)	1.03(9)	0.84(13)

[a]Numbers in parentheses represent uncertainties in last digit(s).
[b]Data taken with cylindrical-mirror analyzer, Ref. 48.
[c]Implanted in Cu. Data taken with HP 5950A ESCA spectrometer.
[d]Total measured linewidth at full width at half-maximum determined by least-squares fit includes instrumental and exciting radiation widths.
[e]Intrinsic width of hole state. Instrumental and radiation widths have been removed by procedures described in Ref. 49.
[f]Total Gaussian component of experimental (Expt) width including instrumental contributions assuming intrinsic width of hole state in gas phase.
[g]Additional Gaussian component not including instrumental width.

may arise from multiple implantation sites associated with the metal lattice, and this possibility is considered in the next subsection. (We should also mention that core-level broadening has been observed in x-ray photoemission spectra of other solid-state materials in which spurious or experimental effects are not present.[53]) Owing to the uncertainty of the exact lattice location of the implanted atoms, however, we cannot rule out experimental effects in these experiments. Nevertheless, we can safely say that lifetime effects associated with interatomic Auger transitions are certainly insignificant compared to this additional broadening. In order for such Auger transitions in the implanted gases to be firmly established, careful analyses of low-kinetic-energy *CVV* Auger spectra must be performed.

Radiation effects

Upon implantation of impurity ions into a target metal, point defects (interstitials and vacancies) and extended defects (dislocations and clusters) are readily formed.[54] A central question to this study is how these defects might affect the interpretation of the observed line shapes and binding-energy shifts. Before attempting to answer this, one must first determine the configuration of the metal atoms with respect to the implanted atom. A wide variety of data has shown that the degree of damage associated with the implantation procedure depends not only on the interactions between implant and target, but also on such factors as the ion dose, the energy of implantation, and the temperature of the target.[55] Specific information about the lattice location of the implanted impurity, which may depend on the target crystal structure and the solubilities and relative sizes of the implanted and target materials, is very scant owing to the limited techniques available for such probing. In view of either the paucity or complexity of the data necessary to answer the question at hand, therefore, some reliance on extrapolation is clearly required.

The average range of the implanted atoms is determined from the theory of Lindhard, Scharff, and Schiott [56](LSS), which predicts average ranges for ions in polycrystalline targets that are in very good agreement with existing experimental data[55,57] and which are reasonably linear with ion-bombardment energies.[58] Extrapolating from this theory to the appropriate ion-energy region in these experiments gives ranges that span from ~20 Å for Ne in Au to ~11 Å for Xe in Au, with similar ranges for Cu and Ag. These values are comparable to the mean escape depth for the photoelectrons investigated.[59] These extrapolated range values are also consistent with our observation that after sequentially sputtering a particular metal target with different rare-gas ions, no evidence was seen in XPS spectra for the previously implanted gases. For example, a sputter yield of ~3 atoms/ion for 1-keV Ar ions[60] bombarding Cu at an ion dose rate of 1.5×10^{13} ions/cm^2 sec corresponds to a removal rate of $\sim 5\times10^{13}$ atoms/cm^2 sec, or about two monolayers per minute. For total ion doses of $\sim10^{16}$ ions/cm^2, about 20 monolayers have been removed, well over the range of these ions.

In addition to the depth profile of the implanted atoms, it is also important to know the damage profile associated with these atoms. To attempt to answer this and related questions, channeling experiments with 1.8-MeV He were performed on single-crystal Cu implanted with Xe under conditions very similar to those in our XPS experiments. The following channeling results were observed: (i) The Xe dose saturated at 2×10^{14} ions/cm^2. (ii) The total damage in the crystal[61] corresponded to a thickness of ~6–7 Å or ~2.5 monolayers of Cu. (iii) There were no orientation effects of the damage in either the ⟨110⟩ or ⟨100⟩ directions. It should

be noted immediately that the channeling technique, which has a depth resolution of ~200 Å and measures only the total number of atoms displaced from channeling directions, is not a very useful probe of short-range-order or near-surface analyses. Nevertheless, some important information is provided by these results.

From the first result, we learn that saturation is easily achieved at the ion doses used, thereby ensuring reasonably reproducible conditions upon minor changes in total dose and sputtering geometry, as observed (see Sec. III B). Assuming the extrapolated LSS *most probable* range for 1-keV Xe in Cu to be correct implies that at least 90% of that Cu lies within twice that range for a Gaussian depth profile. Based on the saturation dose, this implies an average gas concentration of ~1%.

The second result of the channeling experiments suggests that there is, on the average, only a small degree of disorder in the Cu crystal associated with the implanted atoms. At first look this appears to be at most 25% disorder distributed throughout the total range of the implanted gases in the Cu crystal: 6–7 Å is about half the most probable LSS range profile for 1-keV Xe, which, in turn, is about half the total range profile. Upon more careful inspection, however, it is clear that even this picture overestimates the degree of disorder in the crystal. First, it assumes that the implant depth and damage profiles are superimpossible, i.e., collision cascades are unimportant. Second, the total damage or disorder measured in the channeling experiment includes surface contamination on the single crystal, i.e., disorder that is unrelated to the implantation procedure. Therefore, it is safe to conclude that there is only a small amount of disorder in the Cu crystal as a result of implantation. Below we show that this conclusion draws additional support from published calculations and experiments and that from these works, the degree of disorder around the implanted atom may be inferred.

Consider the fate of a gas atom implanted at low energy (< 10 keV) into a metal host in which it is insoluble, as is the case for rare-gas atoms. Much work has shown that there are three most probable processes responsible for the trapping and release, rearrangement, or migration of such gases.[55] The first involves trapping in damage-induced sites whereby rearrangement and/or migration energies of activation less than normal diffusion energy are involved. The second describes trapping to form gas bubbles which migrate depending on the number of vacancies present. Both these mechanisms have been shown to be most important at elevated temperatures and/or high ion-bombardment energies, conditions which are not encountered in these experiments. Some exceptions to this generalization occur for the lighter gases, such as He and Ne, and these will be discussed later on. The third mechanism is one in which the atoms are trapped in sites determined by the repulsive and electronic energies of the atom with the sites in question and in which the atoms migrate according to normal diffusion activation energies. While there is relatively meager experimental data for this process, calculations of energies of solution of He, Ne, Ar, Kr, and Xe in Cu have been performed by Rimmer and Cottrell[62] which predict that substitutional solution for Ar, Kr, and Xe is clearly favorable to interstitial solution. We should point out that the terms "substitutional" and "interstitial" necessarily refer to the atomic configuration of the metal atoms immediately around the implanted atom, not to the bond lengths or positions of these atoms in the normal lattice prior to implantation. This distinction between "substitutional" in this and in the conventional sense is immediately obvious when one considers the relative sizes of the implantation cavity radii (discussed in Sec. IV B) and the Wigner-Seitz radii of the metal hosts: Because the implanted atoms are so much larger, the lattice is expected to distort considerably. In spite of this distortion, however, we do not expect a significant change in the density of nearest-neighbor metal atoms surrounding the implant. Experimental evidence to support this expectation is borne out in a recent Mössbauer channeling study of lattice locations of Xe in Fe (Wigner-Seitz radius of Fe equals that of Cu) in which three different lattice sites—substitutional with none, one, and two vacancies, all in about equal population—were identified.[63] The average number of vacancies associated with each xenon atom, therefore, is only about one out of its eight nearest neighbors. Additional evidence for a relatively uperturbed nearest-neighbor density around the implanted atom is given by thermal-desorption measurements of low-energy Kr in W, from which an upper limit of ~2 vacancies per Kr atom is deduced.[64] It should be noted that this number refers to the vacancies that remain around the implant (many more are initially formed which rapidly diffuse to the surface) and that it does not distinguish between nearest- or next-nearest-neighbors vacancies to the implant. In view of the results of these experiments and calculations, it seems most reasonable to expect that gas atoms implanted in Cu have associated with them only a small fraction of nearest-neighbor vacancies. This over-all description of the implant configuration site is consistent with the results of our channeling experiments, which show that substitutional implantation *in the conventional sense* is not observed [result (iii)] while, at the same time, the total

amount of disorder in the lattice is not very large [result (ii)]. Important to the question at hand, the analysis of binding-energy shifts, is that this description is consistent with our treating the metal-host atoms as a continuous background of positive charge which surrounds the implanted atom. The details of this so-called jellium model have been discussed in Sec. IV.

We may now use the above description to help explain the asymmetric tail observed in the XPS experiments for implanted Ne 1s electrons in Cu, Ag, and Au. This asymmetry is clearly observable and is shown for Ne in Cu in Fig. 6 (a); Fig 6 (b) emphasizes the asymmetry by least-squares fitting only a portion of the raw data. For contrast, this effect should be compared with the symmetric Xe $3d_{5/2}$ line shown in Fig. 5. Although the data in these figures were taken with relatively monochromatic x radiation, the asymmetric line shapes were also observed in data obtained with poorer resolution.[25] We suggest that the origin of this asymmetry most probably lies in the formation of small neon-gas clusters. Experimental evidence to support this comes again from thermal-desorption measurements which show that, in contrast to the larger rare gases implanted at 1 keV, He and Ne desorption follows kinetics predicted by such small-atom clustering.[65] The prominence of clustering increases with increasing ion energy for all the rare gases at the expense of single-atom sites in configurations described above. The description of single- and multiple-atom sites readily explains the observed asymmetry for Ne 1s electrons: A photoionized neon atom in a gas cluster is expected to polarize its immediate environment less efficiently than a single atom surrounded by more mobile metal-conduction electrons. The effect of this reduced screening will be to produce an apparently higher Ne 1s binding energy, as observed.

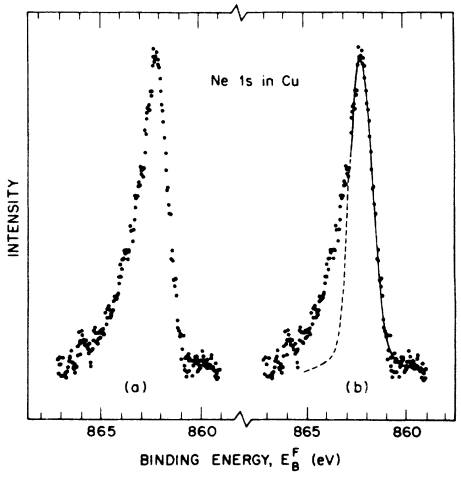

FIG. 6. XPS spectrum of Ne 1s implanted in Cu. (a) Raw data; (b) least-squares fit of fraction of curve (solid line) emphasizing high binding-energy line asymmetry.

APPENDIX B: SOLUTION OF THE THEORETICAL MODEL

The first step in finding the density profile that minimizes the energy functional in either the initial or photoionized condition is to form an Euler-Lagrange differential equation by formally varying the density in Eq. (4). This equation is

$$\frac{c_w}{r}\frac{d^2}{dr^2}(rn^{1/2}) - \tfrac{5}{3}c_k n^{7/6} + \tfrac{4}{3}c_e n^{5/6} + e(V_e + V_{ps} - V_0)n^{1/2} = 0, \qquad \text{(B1)}$$

where V_e and V_{ps} are the electrostatic and pseudopotentials, and V_0 is formally introduced as the Lagrange multiplier associated with the requirement that total particle number be conserved. The total functional actually varied is thus not simply the energy E given in Eq. (4), but

$$F = E + eV_0\int n(\vec{\mathbf{r}})\,d\vec{\mathbf{r}}. \qquad \text{(B2)}$$

The equation has been transformed into the form most suitable for spherical coordinates.

There is a much more physical way to understand the role of V_0. V_{ps} plus V_e as found from Eq. (5) must go to zero far from the origin as a consequence of electrical neutrality. The electron density must go to a constant value n_0 far from the origin, so that in this limit the second derivative in Eq. (B1) must go to zero. From these arguments, it is easy to calculate V_0 from Eq. (B1).

$$eV_0 = \tfrac{4}{3}c_e n_0^{1/3} - \tfrac{5}{3}c_k n_0^{2/3}. \qquad \text{(B3)}$$

Thus V_0 is a density-dependent constant which ensures the proper asymptotic behavior of $n(r)$. However, if we regard the total functional F in Eq. (B2) as a free energy for a system with a variable particle number, eV_0 clearly plays the role of the chemical potential or Fermi level, *measured relative to the average internal electrostatic potential*. Since the photoexcited electron is detected in vacuum, the distinctions between the average internal electrostatic potential, Fermi level, and the vacuum potential must be borne in mind. The expression for the Fermi level given in Eq. (B3) is just that found in the Hartree-Fock-Slater scheme, which is the quantum-mechanical equivalent of the functional method used here.[66]

The conventional self-consistent-field procedure is to guess a starting potential, calculate the charge, find a new potential, and iterate. The charge in the present theory is given by the solution of a nonlinear differential equation whose boundary conditions are that the dependent variable $rn^{1/2}$ vanish at the origin and go to $rn_0^{1/2}$ at infinity. For a given potential, there is no way of assuring that the charge

solution can both satisfy its boundary conditions and yield charge neutrality. Lack of charge neutrality will produce an unacceptable V_e on the next iteration, and so the conventional procedure cannot be followed. Instead, we solve Eqs. (5) and (B1) simultaneously as coupled differential equations. The solutions for n and V_e which satisfy the equations and boundary conditions are then automatically self-consistent.

As a practical matter, it is not possible to satisfy adequately the boundary conditions at infinity by numerical integration alone. An asymptotically exact solution can be found for large r, however, so that numerical integration is needed for only a limited region. To do so, we note that for large r, Eq. (B1) can be linearized by letting $n(r) = n_0 + n_1(r)$, and expanding to first order in n_1/n_0. It then takes the form

$$\frac{d^2}{dr^2}(rn_1) = \left(\frac{20}{9}\frac{c_k}{c_w}n_0^{2/3} - \frac{8}{9}\frac{c_e}{c_w}n_0^{1/3}\right)(rn_1) - \frac{2e}{c_w}n_0[r(V_e + V_{ps})]. \tag{B4}$$

Equations (5) and (B4) form a coupled set of linear differential equations with constant coefficients, and therefore have solutions of the form

$$rn_1 = Ae^{-kr}, \tag{B5}$$

$$rV = (4\pi e/k^2)\,Ae^{-kr}, \tag{B6}$$

where $V = V_e + V_{ps}$, A is an as yet arbitrary amplitude factor, and k is the solution of a quartic equation. The solutions for k for $\epsilon_d = 1$ are

$$a_0k = \pm\left[\frac{2.46}{r_s^2} - \frac{0.407}{r_s} \pm \left(\frac{6.03}{r_s^2} - \frac{14}{r_s} + 0.166\right)^{1/2}\right]^{1/2}, \tag{B7}$$

where a_0 is the Bohr radius and r_s is the Wigner-Seitz electron radius in Bohr units. The argument of the interior square root is negative for $0.43 < r_s < 85$, a range which more than spans all metallic densities, so k is complex and the four solutions for n and V_e are damped sinusoids. The expression for $\epsilon_d > 1$ is qualitatively similar. While it is tempting to draw analogy between these oscillations and Friedel oscillations[67] it is incorrect to do so because these oscillations arise from an interplay between the potential and density rather than from the effect of the sharp Fermi surface. Furthermore, they decay exponentially while Friedel oscillations decay algebraically. It is difficult to anticipate whether an exact self-consistent calculation of an impurity in an electron gas would display such oscillations in the transition between the strongly perturbed small-r range and the large-r Friedel region.

The desired asymptotic solution is a linear combination of two solutions which have a complex-conjugate pair of k's with positive real parts. Thus there is a net amplitude and phase to be determined. These are arbitrary for the linearized equations, but are fixed by the requirement that the asymptotic solution smoothly join the solution of the full nonlinear equation which is integrated numerically from small radius. It has been verified that the solution is highly independent of the joining radius if this radius is chosen so that n_1/n_0 is a few percent or less.

After finding the solutions for n and V_e for a given ion charge and core potential, the functional F is evaluated in a large sphere placed where the charge density has reached n_0 within our numerical accuracy. We will denote this value as $\langle F\rangle$ in analogy with a quantum-mechanical expectation value. A stringent test of our solution and computer codes was performed by holding the repulsive core fixed and increasing the ionic charge by small increments. The relation analogous to the Hellman-Feyman theorem, [68]

$$\frac{d}{d\lambda}\langle F(\lambda)\rangle_\lambda = \left\langle\frac{\partial}{\partial\lambda}F(\lambda)\right\rangle_\lambda, \tag{B8}$$

where λ is the charge strength, was then checked numerically. The left-hand side is computed from the total energy for several values of λ, and the right is equal to the electrostatic potential at the radius of the charge shell for each λ. Agreement was obtained to one in 10^5, which indicates the accuracy of the numerical procedures used.

Having obtained the minimum energies in the initial and photoexcited final states of the system, $\langle F_i\rangle_i$ and $\langle F_f\rangle_f$, we turn to the question of relating these quantities to experimental measurements. [69] We assume that the binding energy of the core state in question is known for the isolated closed-shell atom or ion, and call its magnitude $E_{\rm ref}$. This number includes both the one-electron (Koopmans's theorem[7]) energy of the core state relative to the vacuum, and the polarization energy from all the passive electrons in the outer closed shell and other core states.

For an x ray of energy $\hbar\omega$, the energy of an electron photoemitted from the free atom or ion is given by

$$E_{pe} = \hbar\omega - E_{\rm ref}. \tag{B9}$$

Now suppose we introduce the solid surrounding the reference atom, allow the electrons to adjust to its potential in the initial state, and freeze them in that configuration. The photoemitted electron will now have its energy shifted because of the potential produced by the other electrons and ions. Its energy is now given, in terms of our theory, by

$$E_{pe} = \hbar\omega - E_{\rm ref} + \langle F_i\rangle_i - \langle F_f\rangle_i, \tag{B10}$$

where $\langle F_f\rangle_i$ indicates that the final-state pseudopo-

tential is used but the energy functional is evaluated for that charge distribution which minimizes the functional with the initial-state pseudopotential. A moment's reflection indicates that E_{pe} must be measured *relative to the average electrostatic potential inside the solid* for Eq. (B10) to be valid.

Further energy can be gained by allowing the electron distribution to relax to accommodate itself to the final state pseudopotential. We will assume that all this energy gets transferred to the photoelectron, while recognizing the fact that incomplete relaxation can, in principle, add a tail to the low energy side of the observed line. With the relaxation energy included, we find

$$E_{pe} = \hbar\omega - E_{\rm ref} + [\langle F_i\rangle_i - \langle F_f\rangle_i] + [\langle F_f\rangle_i - F_f\rangle_f], \quad \text{(B11)}$$

which simply reduces to

$$E_{pe} = \hbar\omega - E_{\rm ref} + \langle F_i\rangle_i - \langle F_f\rangle_f. \quad \text{(B12)}$$

It is thus seen that while the separation into potential shift and relaxation or polarization energy is conceptually useful, it is inessential in terms of the actual evaluation of the photoelectron energy from our theory.

The energy given in Eq. (B12) is still referred to the average internal potential, which is a theoretically convenient but experimentally inaccessible number. The two useful references are the vacuum level and the Fermi level. The photoelectron energies in terms of these references are

$$E_{pe}^{V} = \hbar\omega - E_{\rm ref} + \langle F_i\rangle_i - \langle F_f\rangle_f - eD, \quad \text{(B13)}$$

$$E_{pe}^{F} = \hbar\omega - E_{\rm ref} + \langle F_i\rangle_i - \langle F_f\rangle_f - eV_0, \quad \text{(B14)}$$

where D is the surface dipole potential (defined to be positive when the electron must climb a potential barrier to get out), and V_0 is given by Eq. (B1). The difference between Eqs. (B13) and (B14) is, of course, the work function. Which equation it is better to use for comparison with experiment depends on the relative confidence in our ability to calculate V_0 versus our ability to calculate D.

[1]S. B. M. Hagström, C. Nordling, and K. Siegbahn, Phys. Lett. 9, 235 (1964); Z. Phys. 178, 439 (1964).
[2]K. Siegbahn, C. Nordling, A. Fahlman, R. Nordberg, K. Hamrin, J. Hedman, G. Johansson, T. Bergmark, S.-E. Karlsson, I. Lindgren, and B. Lindberg, *ESCA-Atomic, Molecular and Solid State Structure by Means of Electron Spectroscopy* (Almqvist and Wicksells, Uppsala, Sweden, 1967).
[3]K. Siegbahn, C. Nordling, G. Johansson, J. Hedman, P. F. Hedén, K. Hamrin, U. Gelius, T. Bergmark, L. O. Werme, R. Manne, and Y. Baer, *ESCA Applied to Free Molecules* (North-Holland, Amsterdam, 1969).
[4]Y. S. Khodeyev, H. Siegbahn, K. Hamrin, and K. Siegbahn, Chem. Phys. Lett. 19, 16 (1973).
[5]H. Siegbahn and K. Siegbahn, J. Electron Spectro. 2, 319 (1973).
[6]U. Gelius, E. Basilier, S. Svensson, T. Bergmark, and K. Siegbahn, J. Electron Spectro. 2, 405 (1973).
[7]T. Koopmans, Physica (Utr.) 1, 104 (1933).
[8]A. Surea and G. Berthier, J. Phys. 24, 672 (1963).
[9]P. S. Bagus, Phys. Rev. 139, A619 (1965).
[10]I. Lindgren, Ark. Fys. 31, 59 (1965).
[11]M. A. Coulthard, Proc. Phys. Soc. Lond. 91, 44 (1967).
[12]A. Rosén and I. Lindgren, Phys. Rev. 176, 114 (1968).
[13]F. A. Gianturco and C. A. Coulson, Molec. Phys. 14, 223 (1968).
[14]C. M. Moser, R. K. Nesbet, and G. Verhaegen, Chem. Phys. Lett. 12, 230 (1971).
[15]U. Gelius, G. Johansson, H. Siegbahn, C. J. Allan, D. A. Allison, J. Allison, and K. Siegbahn, J. Electron Spectro. 1, 285 (1973).
[16]H. Basch and L. C. Snyder, Chem. Phys. Lett. 3, 333 (1969).
[17]M. E. Schwartz, Chem. Phys. Lett. 5, 50 (1970).
[18]I. H. Hillier, V. R. Saunders, and M. H. Wood, J. Chem. Phys. 7, 323 (1970).
[19]C. R. Brundle, M. B. Robin, and H. Basch, J. Chem. Phys. 53, 2196 (1970).
[20]R. Moccia and M. Zandomeneghi, Chem. Phys. Lett. 11, 221 (1971).
[21]P. S. Bagus and H. F. Schaeffer III, J. Chem. Phys. 55, 1474 (1971).
[22]D. T. Clark and D. B. Adams, J. Electron Spectro. 1, 302 (1973).
[23]L. Hedin, Ark. Fys. 30, 231 (1965).
[24](a) P. H. Citrin, R. W. Shaw, Jr., A. Packer, and T. D. Thomas, *Electron Spectroscopy*, edited by D. A. Shirley (North-Holland, Amsterdam, 1972), p. 691; (b) P. H. Citrin and T. D. Thomas, J. Chem. Phys. 57, 4446 (1972).
[25]P. H. Citrin and D. R. Hamann, Chem. Phys. Lett. 22, 301 (1973).
[26]G. Johansson, J. Hedman, A. Berndtsson, M. Klasson, and R. Nilsson, J. Electron Spectro. 2, 295 (1973).
[27]D. E. Eastman, Phys. Rev. B 2, 1 (1970).
[28]M. L. Cohen and V. Heine, in *Solid State Physics*, edited by H. Ehrenreich, F. Seitz, and D. Turnbull (Academic, New York, 1970), Vol. 24, p. 38.
[29]L. Hedin and G. Johannson, J. Phys. B 2, 1336 (1969).
[30]D. A. Shirley, Chem. Phys. Lett. 16, 220 (1972).
[31]L. Ley, S. P. Kowalczyk, F. R. McFeely, R. A. Pollak, and D. A. Shirley, Phys. Rev. B 8, 2392 (1973).
[32]P. Gombás, in *Handbuch der Physik*, edited by S. Flügge (Springer, Berlin, 1956), Vol. 36, p. 109.
[33]A. Meyer, I. H. Umar, and W. H. Young, Phys. Rev. B 4, 3287 (1971).
[34]C. F. V. Weizsäcker, Z. Phys. 96, 431 (1935).
[35]N. W. Ashcroft, Phys. Lett. 23, 48 (1966).
[36]D. G. Thompson, J. Phys. B 4, 468 (1971).
[37]G. Kienast and J. Verma, Z. Anorg. Allgem. Chem. 310, 143 (1961).
[38]H. Ehrenreich and H. R. Phillips, Phys. Rev. 128, 1622 (1962).
[39]D. R. Penn, Phys. Rev. 128, 2093 (1962).
[40]P. B. Johnson and R. W. Christy, Phys. Rev. B 6, 4370 (1972).
[41]N. D. Lang and W. Kohn, Phys. Rev. B 3, 1215 (1971).

[42]J. A. Appelbaum and D. R. Hamann, Phys. Rev. B 6, 1122 (1972).
[43]P. H. Citrin and D. R. Hamann (unpublished).
[44]W. Bambynek, B. Crasemann, R. W. Fink, H.-U. Freund, H. Mark, C. D. Swift, R. E. Price, and P. V. Rao, Rev. Mod. Phys. 44, 716 (1972).
[45]R. W. Shaw, Jr. and T. D. Thomas, Phys. Rev. Lett. 29, 689 (1972).
[46]R. M. Friedman, J. Hudis, and M. L. Perlman, Phys. Rev. Lett. 29, 692 (1972).
[47]P. H. Citrin, Phys. Rev. Lett. 31, 1164 (1973).
[48]P. H. Citrin, R. W. Shaw, Jr., and T. D. Thomas, in *Electron Spectroscopy*, edited by D. A. Shirley (North-Holland, Amsterdam, 1972), p. 105.
[49]The linewidths measured with the cylindrical-mirror analyzer were assumed to be a convolution of (a) a Lorentzian width intrinsic to the hole state, (b) a Lorentzian component due to the exciting Al $K\alpha$ radiation, and (c) a Gaussian spectrometer component of width ΔE. This latter width, which depends on the kinetic energy of the nonretarded photoelectrons, is empirically determined from gas-phase measurements of Ne 1*s* and Ne $KLL(^1D)$ electrons assuming an intrinsic Ne 1*s* width of 0.26 eV (Ref. 50). The Al $K\alpha_{1,2}$ doublet, whose components are assumed to be 2:1 in intensity, split by 0.44 eV (Ref. 51), and each of width 0.35 eV (0.33 eV for the 1*s* width, Ref. 50, and 0.02 eV for the $2p_{3/2,1/2}$ width, Ref. 52) is approximated by a single Lorentzian peak of width 0.60 eV. The intrinsic width of the hole state is determined by convoluting the above functions with varying Lorentzian widths until the measured width is obtained. A similar procedure is used for the implanted-gas data assuming the total measured width is composed of a Lorentzian "intrinsic" width convoluted with a Gaussian spectrometer function of 0.60-eV width. This latter value was determined from Gaussian smearing of thermally broadened Fermi edges of various metals.
[50]E. J. McGuire, Phys. Rev. 185, 1 (1969).
[51]C. E. Moore, *Atomic Energy Levels*, Natl. Bur. Std. Circ. No. 467 (U. S. GPO, Washington, D. C., 1949).
[52]T. Kobyasi and A. Morita, J. Phys. Soc. Jpn. 28, 457 (1970).
[53]P. H. Citrin, P. Eisenberger, and D. R. Hamann, Phys. Rev. Lett. 33, 965 (1974).
[54]See, for example, M. W. Thompson, *Defects and Radiation Damage in Metals* (Cambridge U. P., London, 1969).
[55]See, for example, G. Carter and J. S. Collington, *Ion Bombardment of Solids* (Elsevier, New York, 1968).
[56]J. Lindhard, M. Scharff, and H. E. Schiott, Kgl. Danske Videnskab. Selskab, Mat.-Fys. Medd. 33, No. 14 (1963).
[57]See, for example, T. Jokić, Phys. Status Solidi A 18, K77 (1973).
[58]W. S. Johnson and J. F. Gibbons, *Projected Range Statistics in Semiconductors* (Stanford U. P., Palo Alto, Calif., 1969).
[59]See, for example, J. C. Tracy, in *Electron Emission Spectroscopy*, edited by W. Dekeyser, L. Fiermans, G. Vanderkelen, and J. Vennik (D. Reidel, Boston, Mass., 1973), p. 305.
[60]G. Carter and J. S. Collington, in Ref. 55, p. 314.
[61]The "damage" due to the surface layer is not included.
[62]D. E. Rimmer and A. H. Cottrell, Philos. Mag. 2, 1345 (1957).
[63]H. deWaard and L. C. Feldman, in *Proceedings of the International Conference on Applied of Ion Beams to Metals* (Plenum, New York, 1974).
[64]E. V. Kornelsen, Radiat. Eff. 13, 227 (1972); and private communication.
[65]E. V. Kornelsen and M. K. Sinha, Can. J. Phys. 46, 613 (1968).
[66]J. C. Slater, Phys. Rev. 81, 385 (1951).
[67]J. Friedel, Philos. Mag. Suppl. 3, 446 (1954).
[68]H. Hellmann, *Einfuhrung in die Quantenchemie*, (Franz Denticke, Liepzig and Vienna, 1937), Sec. 1-2; R. P. Feynman, Phys. Rev. 56, 340 (1939).
[69]By using the "free energy" F, Eq. (B2), rather than the energy E, we avoid having to explicitly include the initial-state energy of the electron brought in to screen the core hole.